

Chemical Science

Accepted Manuscript

This article can be cited before page numbers have been issued, to do this please use: R. Yagami, W. Xu, T. Kobayashi, Y. Nagata and N. Kumagai, *Chem. Sci.*, 2025, DOI: 10.1039/D5SC02937F.



This is an Accepted Manuscript, which has been through the Royal Society of Chemistry peer review process and has been accepted for publication.

Accepted Manuscripts are published online shortly after acceptance, before technical editing, formatting and proof reading. Using this free service, authors can make their results available to the community, in citable form, before we publish the edited article. We will replace this Accepted Manuscript with the edited and formatted Advance Article as soon as it is available.

You can find more information about Accepted Manuscripts in the [Information for Authors](#).

Please note that technical editing may introduce minor changes to the text and/or graphics, which may alter content. The journal's standard [Terms & Conditions](#) and the [Ethical guidelines](#) still apply. In no event shall the Royal Society of Chemistry be held responsible for any errors or omissions in this Accepted Manuscript or any consequences arising from the use of any information it contains.

ARTICLE

***iso*-TEtraQuinoline (*i*-TEQ): An Inherently Chiral N4 Macrocyclic Quinoline Tetramer**Ryota Yagami,^{a,*} Wei Xu,^{a,*} Toi Kobayashi,^a Yuuya Nagata,^b Naoya Kumagai^{a,c,*}Received 00th January 20xx,
Accepted 00th January 20xx

DOI: 10.1039/x0xx00000x

Chiral macrocycles are attracting growing interest due to their broad applicability as ligands in asymmetric catalysis and as host molecules for chiral recognition. Robustness and high thermodynamic stability can be effectively achieved by strategically linking aromatic panels to construct an axially chiral macrocyclic framework. Cyclic concatenation of four quinoline units affords a fully sp^2 -hybridized, non-planar macrocycle featuring four inwardly oriented, coordinatively active pyridyl nitrogen atoms. The previously reported tetramer TEtraQuinoline (TEQ) exhibits head-to-tail connectivity of its quinoline units, affording an achiral architecture possessing S_4 symmetry. Herein, we report the design and synthesis of *iso*-TEtraQuinoline (*i*-TEQ), an inherently chiral analogue featuring head-to-head connectivity at the 2,2'- and 8,8'-positions, which gives rise to a D_2 -symmetric architecture. Detailed comparative investigations of the connectivity isomers *i*-TEQ and TEQ revealed an array of distinct characteristics, including the overall architecture, intrinsic macrocyclic strain, spatial orientation of nitrogen lone pairs, thermodynamic stability, racemisation behaviour, metal complex stability, and circularly polarised luminescence.

Introduction

The chemical space occupied by axially chiral entities has remarkably expanded over the past several decades owing to their diverse applications as chiral ligands,¹ chiral sensing materials,² and biologically active natural or artificial products.³ Due to their high thermodynamic stability and structural robustness, axially chiral molecules composed of sp^2 -hybridized aromatic units have attracted considerable attention for the construction of well-defined chiral environments in catalysis and sensing applications. The 1,1'-binaphthyl unit represents a privileged scaffold for this purpose and is extensively utilized in catalyst design by incorporating chalcogen and pnictogen atoms at 2,2'-positions to promote enantioselective metal- and organocatalysis, and molecular recognition⁴ (Fig. 1a). In contrast, the 8,8'-biquinoline framework, which is structurally analogous to the 1,1'-binaphthyl but features an N(sp^2) atom in place of one C(sp^2)–H unit, is utilized only sparingly due to its relatively low racemisation barrier⁵ (Fig. 1b). Incorporating the quinoline unit

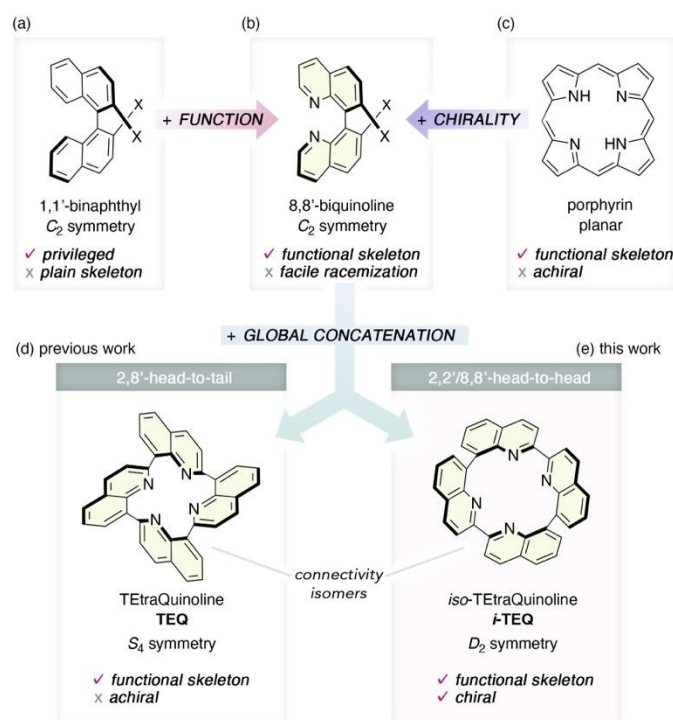


Fig. 1 Hierarchical structural modulation with respect to axial chirality and intrinsic functionality. (a–c) Structure and properties of 1,1'-binaphthyl, 8,8'-biquinoline, and porphyrin. (d) Previously studied TEtraQuinoline (TEQ) and its architectural features. (e) The newly developed macrocyclic quinoline framework, *iso*-TEtraQuinoline (*i*-TEQ), embodies both intrinsic functionality and inherent chirality.

^a Graduate School of Pharmaceutical Sciences, Keio University
1-5-30 Shibakoen, Minato-ku, Tokyo 105-8512, Japan
E-mail: kumagai-ny@keio.jp

^b Institute for Chemical Reaction Design and Discovery (WPI-ICReDD),
Hokkaido University, Hokkaido Kita 21, Nishi 10, Kita-ku, Sapporo, Hokkaido
001-0021, Japan

^c Institute of Microbial Chemistry
3-14-23 Kamiosaki, Shinagawa-ku, Tokyo 141-0021, Japan

Electronic Supplementary Information available: [details of any supplementary information available should be included here]. See DOI: 10.1039/x0xx00000x

*These authors contributed equally.



is particularly advantageous, as it not only imparts axially chirality but also introduces a functional motif capable of coordinating metal cations, thereby offering dual functionality in a single framework. Inspired by porphyrin—a representative functional framework ubiquitous in nature that coordinates metal cations through four sp^2 -hybridized nitrogen atoms—we previously designed a tetrameric quinoline construct, TEtQuinoline (TEQ), as a non-planar analogue of porphyrin.⁶ While its cyclic concatenation effectively suppresses the flipping of the linked quinoline units, the head-to-tail assembly through the 2- and 8-positions imparts an overall achiral, S_4 -symmetric rigid architecture to the TEQ framework. Given the diverse chemistry exhibited by TEQ in metal coordination, photophysical behaviour, and catalytic applications,⁷ the development of its chiral variant is highly desirable. Herein, we report the re-design of a quinoline-based, axially chiral molecular framework that functions as a tetradentate nitrogen ligand: *iso*-TEtQuinoline (*i*-TEQ).⁸ By switching the ring connectivity from head-to-tail to head-to-head at the 2,2'- and 8,8'-positions, *i*-TEQ adopts a D_2 -symmetric, inherently chiral architecture.⁹ Detailed comparative structural analyses uncovered similarities and differences between these connectivity isomers, highlighting the impact of the concatenation pattern on the chemical and photophysical properties.

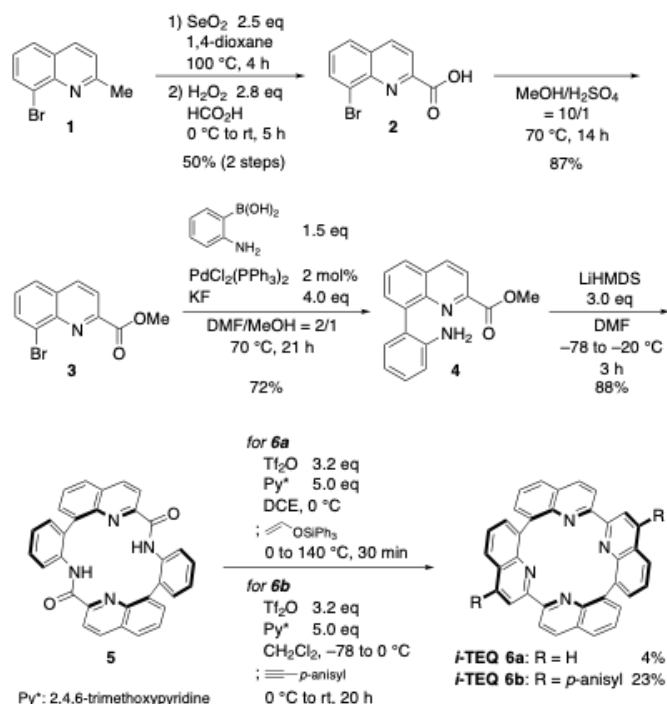
Results and Discussion

Synthesis of *iso*-TEtQuinolines (*i*-TEQs)

Inspired by the TEQ framework, we designed a synthetic plan utilizing cyclic diamide **5** with two quinoline units as a

key precursor to *i*-TEQ via a two-fold quinoline forming reaction (Scheme 1). The synthesis of *i*-TEQ was initiated by a two-step benzylic oxidation of 8-bromo-2-methylquinoline **1** mediated by SeO_2 and H_2O_2/HCO_2H to afford carboxylic acid **2**. After converting **2** into methyl ester **3** with H_2SO_4 in MeOH, Suzuki-Miyaura cross-coupling with (2-amino)phenylboronic acid afforded aminoester **4**.¹⁰ Following brief screening,¹¹ simple cryogenic and highly diluted conditions with LiHMDS engaged **4** in smooth amidative dimerization, furnishing the requisite cyclic diamide **5** in 88% yield. According to Movassaghi's protocol¹² and our previous modification for quinoline formation from macrocyclic amides,^{6a,h,i} electrophilic activation of the amide functionality using Tf_2O and 2,4,6-trimethoxypyridine and subsequent formal cycloaddition afforded the *i*-TEQ architecture. Quinoline formation with (triphenylsiloxy)ethylene furnished non-substituted D_2 -symmetric *i*-TEQ **6a**, but the yield was only 4%. More reactive *p*-anisylacetylene allowed for a more efficient ring reinforcement reaction to give C_2 -symmetric bis-*p*-anisylated *i*-TEQ **6b** in 23% yield. The *p*-anisyl groups of *i*-TEQ **6b** can be smoothly demethylated, enabling further structural elaboration.¹³

A detailed comparative structural analysis was performed on the thus-obtained *i*-TEQ **6b**—a connectivity isomer of *p*-anisylated TEQ **7b** sharing the same atomic composition (Fig. 2). To minimize structural deviations caused by crystal packing effects, DFT-optimized structures of both isomers were compared using the B3LYP-D3/6-31G(d,p) level of theory with the IEFPCM($CHCl_3$) solvation model (Fig. 2a).¹⁴ Comparison of the top views of these structures revealed a distinct difference in the inner hollow topology: *i*-TEQ **6b** features a diamond-shaped 16-membered macrocycle, while TEQ **7b** exhibits a square-like counterpart. In contrast, the spatial arrangement of the four nitrogen atoms is similar, with the distances between diagonal nitrogen atoms being nearly identical, ranging from 4.35 to 4.47 Å. Additionally, the τ_4 values¹⁵ are close to zero, suggesting that *i*-TEQ **6b**, like TEQ **7b**, is capable of accommodating metal cations that prefer a square planar coordination mode (Fig. 2a,b). The diamond-shaped cavity of *i*-TEQ **6b** arises from the head-to-head (2,2' and 8,8') linkage of the quinoline units, leading to an overall laterally distorted structure characterized by reduced dihedral angles and an increased vertical dimension (*i*-TEQ **6b**: 6.56 Å vs TEQ **7b**: 6.01 Å). Whereas the D_2 -symmetric *i*-TEQ skeleton is more stable than the S_4 -symmetric TEQ skeleton ($\Delta G = 2.2$ kcal·mol⁻¹), enthalpic evaluation *via* a homodesmotic reaction¹⁶ and StrainViz analysis¹⁷ indicated that *i*-TEQ adopts a more strained architecture (difference in total strain: 9.0 kcal·mol⁻¹), with the local structures of the intrinsic quinoline units being more distorted (Fig. 2b–d). This seemingly contradictory outcome is attributed to electronic repulsion between the lone pairs on the inwardly oriented nitrogen atoms; those of *i*-TEQ are oriented in a mutually more skewed fashion to prevent undesired overlapping. This electronic factor likely outweighs the skeletal distortion, rendering *i*-TEQ more thermodynamically stable than TEQ, as supported by TG-DTA analysis; *i*-TEQ **6b** remains stable above 300 °C, whereas TEQ **7b** begins to decompose above 250 °C.¹⁸



Scheme 1 Synthesis of *i*-TEQ **6a,b**.



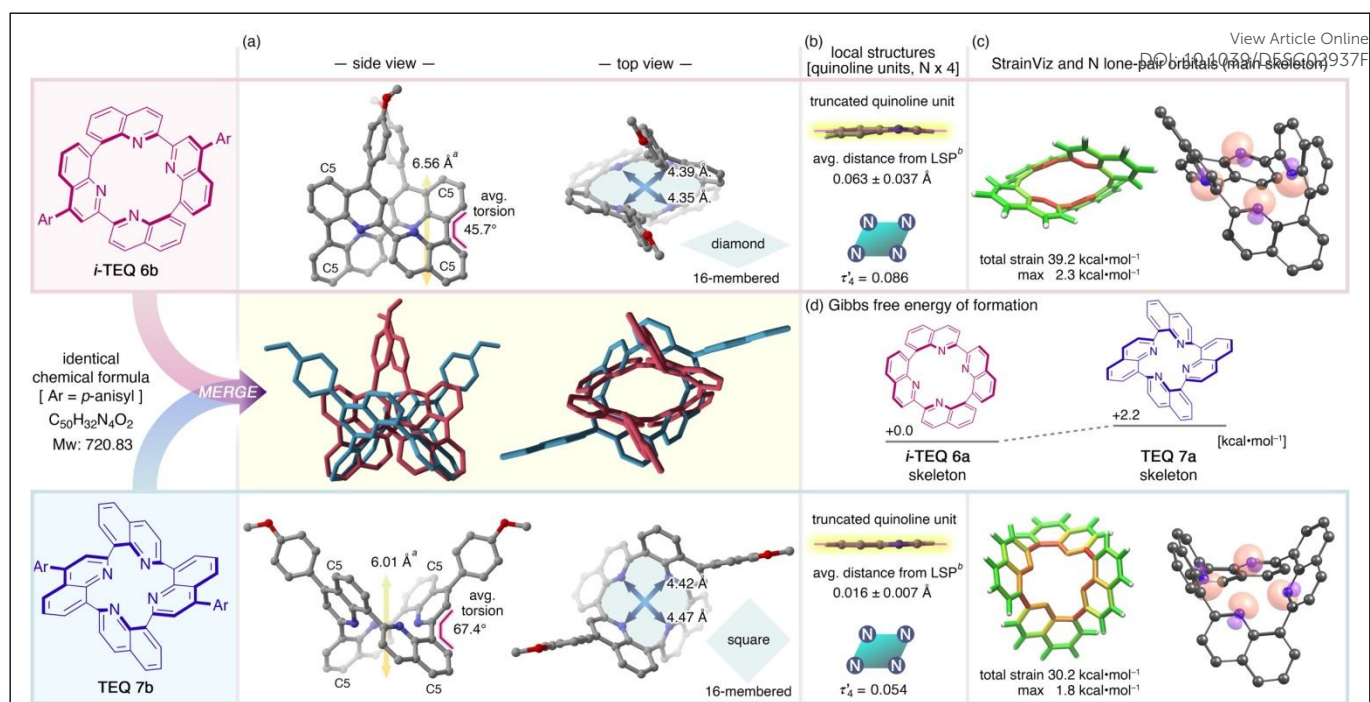


Fig. 2 Structural comparison of connectivity isomers *i*-TEQ 6b and TEQ 7b sharing a tetrameric quinoline macrocyclic architecture and two peripheral diagonal *p*-anisyl groups. (a) Optimized structures are calculated at the B3LYP-D3/6-31G(d,p)/IEFPCM(CHCl₃) level of theory. Colour codes; carbon: grey, nitrogen: blue, oxygen: red, hydrogen atoms are omitted for clarity. ^aVertical size of the main framework is calculated by the distance between the midpoint of the two quinoline C5 carbons on the upper side and the midpoint of the two quinoline C5 carbons on the lower side. (b) Analysis of local structures. ^bLSP: least squares plane. More detailed analysis is summarized in Supplementary Information. (c) StrainViz analysis and NBO of nitrogen lone pairs. StrainViz calculation was carried out at the B3LYP/6-31G(d) level of theory. (d) Comparison of Gibbs free energy for the formation of non-substituted *i*-TEQ 6a and TEQ 7a.

Physicochemical properties of *i*-TEQs

The structural rigidity of the *i*-TEQ framework, a cyclic assembly of four quinoline panels with a hitherto unknown pattern of connectivity, is great of interest. Racemic samples of *D*₂-symmetric non-substituted *i*-TEQ 6a and *C*₂-symmetric *p*-anisylated *i*-TEQ 6b were optically resolved *via* preparative HPLC on a chiral stationary phase (Fig. 3a). 6a and 6b were successfully resolved with base-peak separation under identical conditions (DAICEL CHIRALPAK IB-N5, ⁿhexane/CH₂Cl₂ mixed solvent eluent). The initially eluted enantiomers of both 6a and 6b displayed a positive Cotton effect in a range of 330–350 nm, corresponding to HOMO–LUMO excitation (Fig. 3b).¹⁹ DFT simulations of electronic CD spectra suggested the absolute configuration shown in Fig. 3a.²⁰ Intriguingly, optical rotation of the first eluents of 6a and 6b were opposite (6a: dextrorotatory, 6b: levorotatory), presumably because the closely located diagonal *p*-anisyl groups of 6b affected optical rotation at the wavelength of sodium D-lines.

The stereochemical integrity of (–)-*i*-TEQ 6b was traced at a 1 mg/mL concentration in diphenyl ether under various conditions (Table 1). The initial racemisation attempt without any additive confirmed that the stereochemistry of the *i*-TEQ architecture is quite stable; no decomposition or erosion of enantiopurity was observed even at 220 °C for 24 h (Entry 1). DFT calculations on the non-substituted *i*-TEQ 6a successfully reproduced the experimentally observed high racemisation barrier, yielding an inversion barrier of

62.0 kcal·mol⁻¹ for the transition state at the B3LYP-D3/6-31G(d,p) level of theory (Fig. 4a). Given that structurally similar acyclic azaBINOL is readily racemised (28.4 kcal·mol⁻¹),^{5a} the unusual retention of axial chirality of *i*-TEQ is likely due to its unique concatenated structure. Notably, the inversion barrier of *i*-TEQ 6a is

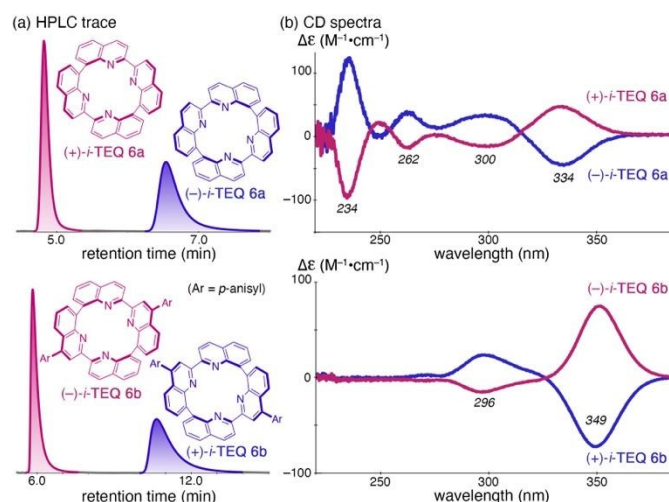
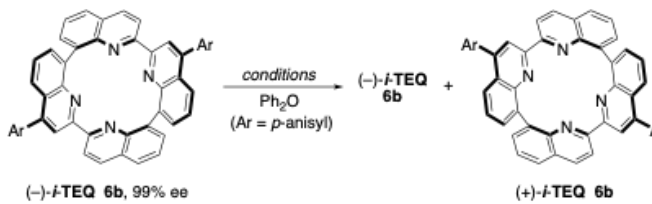


Fig. 3 (a) Partial HPLC chromatogram for optical resolution of *rac*-*i*-TEQ 6a and 6b separated by DAICEL CHIRALPAK IB-N5 column with ⁿhexane/CH₂Cl₂ eluent. (b) Circular dichroism (CD) spectra of optically pure samples of non-substituted (+)- and (–)-*i*-TEQ 6a, and anisylated (+)- and (–)-*i*-TEQ 6b in CH₂Cl₂ (25 μM).



Table 1. Racemisation study of *i*-TEQ **6b** in the absence or presence of additives



Chemical reaction scheme showing the racemisation of **(-)-i-TEQ 6b** to **(+)-i-TEQ 6b** under conditions in Ph_2O ($\text{Ar} = p\text{-anisyl}$).

Entry	Additive ^a	Temp. (°C)	Time (h)	ee ^b (%)	Rate constant (x 10 ⁻⁷ s ⁻¹)	t _{1/2} (h)	ΔG [‡] _{exp} (kcal·mol ⁻¹)	ΔG [‡] _{calc} ^c (kcal·mol ⁻¹)
1	none	220	24	>99	— ^d	—	—	58.0
2	TFA	140	24	>99	— ^d	—	—	50.8 ^e , 46.3 ^f
3		160	56	91	2.18	883	38.9	
4	[Pd(MeCN) ₄](BF ₄) ₂	100	30	63	20.2	95.3	31.8	33.3
5		140	2.5	20	888	2.2	32.1	
6	CoCl ₂	100	24	>99	— ^d	—	—	30.6
7		140	56	88	2.99	644	36.8	
8	CuCl ₂	100	24	>99	— ^d	—	—	34.4
9		140	30	72	14.8	130	35.5	

^a1 equivalent of additives was added. ^bDetermined by chiral stationary phase HPLC analysis. ^cΔG[‡]_{calc} was calculated on non-substituted *i*-TEQ **6a** at the B3LYP-D3/6-311+G(2d,p)-SDD(Co,Cu,Pd)/SMD(diethyl ether) level of theory. Compared with Fig. 4, a more extended basis set was employed and an appropriate solvation model was applied. ^dNo racemisation occurred. ^eCalculated on the monoprotonated model. ^fCalculated on the diprotonated model.

even higher than that of the configurationally stable TEQ **7a** (56.9 kcal·mol⁻¹), and the inversion process proceeds via a stepwise mechanism involving a C_i-symmetric intermediate, in contrast to the single-step flipping observed for TEQ **7a** (Fig. 4a). We reasoned that mitigating the repulsive orbital interactions of the four inwardly oriented nitrogen atoms enhanced the racemisation. While racemisation of (–)-*i*-TEQ **6b** barely proceeded in the presence of 1 equivalent of trifluoroacetic acid (TFA) at 140 °C, a higher temperature (160 °C) induced slow the racemisation (t_{1/2} = ca. 37 days) (Table 1, Entries 2,3). Quinoline ring flipping was significantly accelerated by the addition of [Pd(MeCN)₄](BF₄)₂ with t_{1/2} of 2.2 h at 140 °C (20% ee after 2.5 h), which corresponds to an empirically determined flipping barrier of 32.1 kcal·mol⁻¹ (Entries 4,5). Intriguingly, *p*-anisylated (–)-TEQ **7b**, featuring head-to-tail concatenation, was significantly more reluctant to racemise and remained at 88% ee even after 24 h of stirring under identical conditions (with Pd salt at 140 °C).²¹ This distinct response to the Pd²⁺ cation was reproduced by DFT calculations (Fig. 4b); the pathway

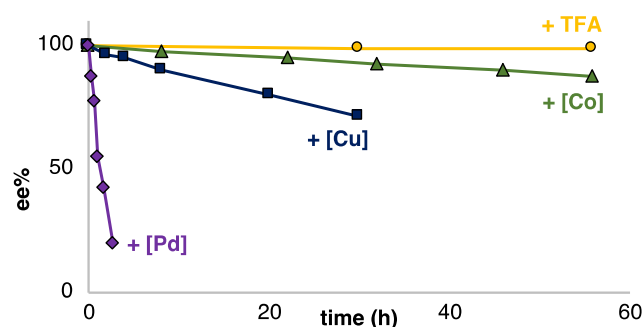
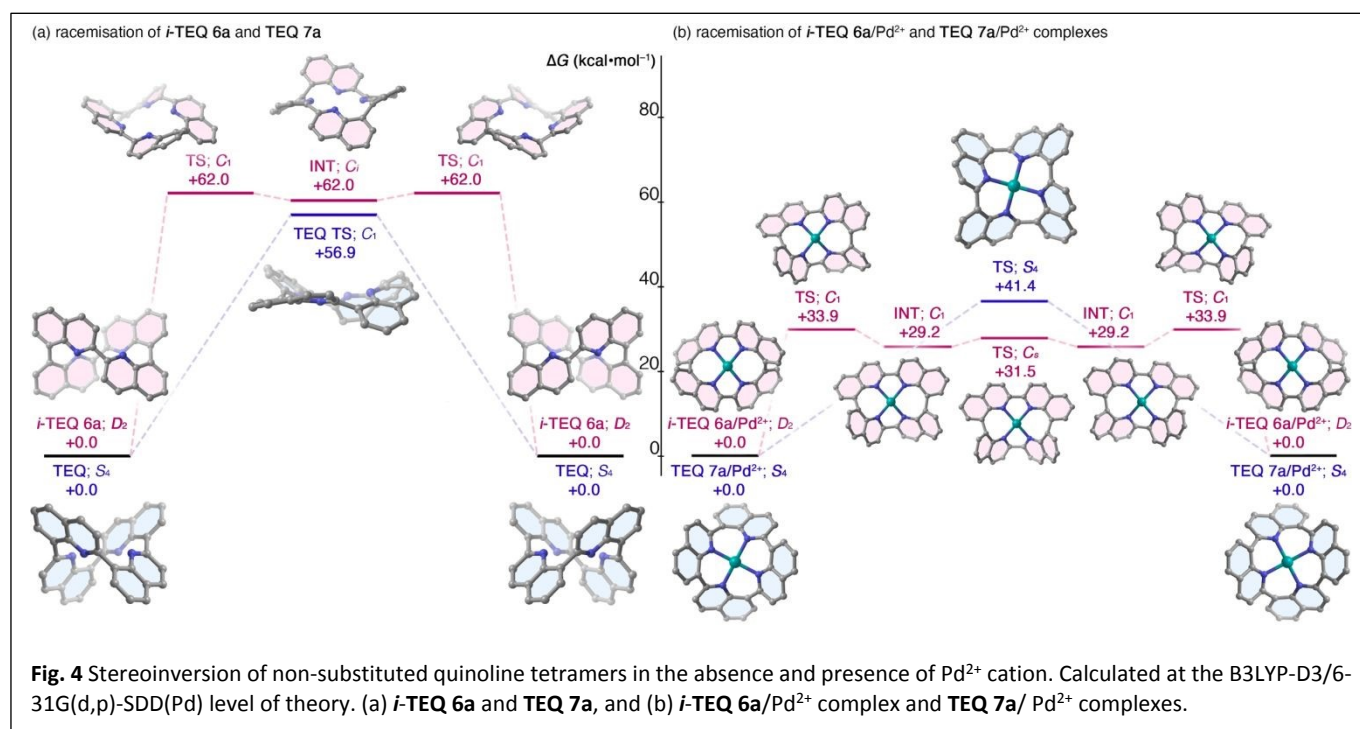


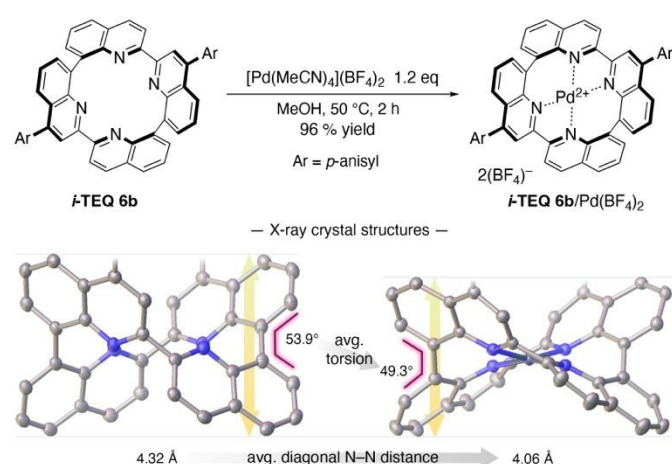
Fig. 5 Racemisation profile of enantiopure (–)-*i*-TEQ **6b** in the presence of additives (1 eq) at 140 °C in diphenyl ether (1 mg/mL). A plot of enantiomeric excess (%) versus time is shown. Enantiomeric excess was determined by chiral stationary phase HPLC analysis.



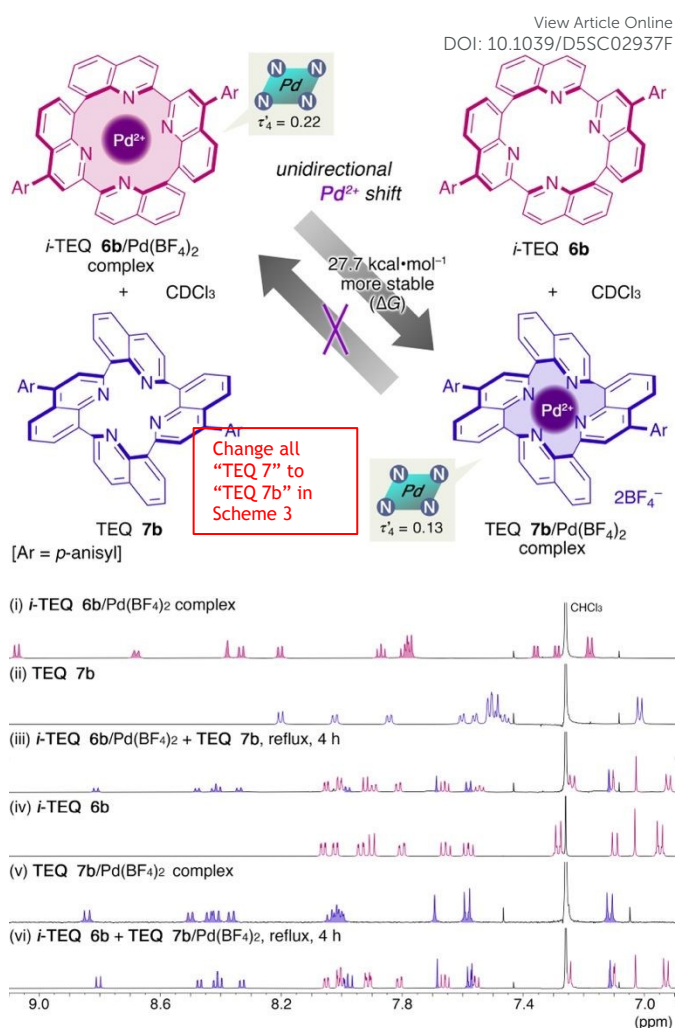
from the *i*-TEQ **6a**/Pd²⁺ complex to its antipode involves a series of local minima connected by partially flipped C₁- and C₂-symmetric transition states, which significantly lower the inversion barrier. In contrast, the TEQ **6a**/Pd²⁺ complex undergoes a high-energy S₄-symmetric transition state to achieve stereoinversion. Other azophilic metal cations featuring a square planar coordination mode, e.g. Co²⁺ or Cu²⁺ rendered racemisation, whereas acceleration was significantly smaller than that of Pd²⁺ and no racemization occurred at a temperature not exceeding 100 °C (Table 1, Entries 6–9). A plot of enantiomeric excess and elapsed time clearly demonstrates the substantial rigidity and characteristic response to Pd²⁺ in the racemisation of (–)-*i*-TEQ **6b** (Fig. 5). DFT calculations located energetically more favourable transition states by protonation or metal coordination.²²

The accelerated racemisation of (–)-*i*-TEQ **6b** in the presence of Pd²⁺ demonstrates that *i*-TEQ is capable of accommodating Pd²⁺ cations despite the highly twisted configuration of the lone pair orbitals of the four quinoline nitrogen atoms (Fig. 2c). Indeed, treatment of *i*-TEQ **6b** with [Pd(MeCN)₄](BF₄)₂ in MeOH at 50 °C furnished the *i*-TEQ **6b**/Pd(BF₄)₂ complex in excellent yield (Scheme 2). Comparative X-ray diffraction analysis of the crystal structures of *i*-TEQ **6b** and *i*-TEQ **6b**/Pd(BF₄)₂ revealed that both the averaged torsion angle at 8,8'-biquinoline units and the averaged distance of the diagonal nitrogen atoms decreased upon complexation from 53.9° to 49.3° and from 4.32 to 4.06 Å, respectively, leading to a vertically collapsed architecture.

To probe the thermodynamic stability of the Pd²⁺ complexes of *i*-TEQ **6b** and TEQ **7b**, structural isomers with an identical elemental composition, a ligand metathesis experiment was conducted (Scheme 3). The *i*-TEQ **6b**/Pd(BF₄)₂ complex and metal-free TEQ **7b** were mixed in CDCl₃ and heated under reflux. ¹H NMR revealed that the signals derived from both the *i*-TEQ **6b**/Pd(BF₄)₂ complex and the TEQ **7b** completely disappeared (Scheme 3, (i,ii) vs (iii)). Instead,



Scheme 2. Complexation of *i*-TEQ **6b** with [Pd(MeCN)₄](BF₄)₂, and crystal structures of the **6b** and **6b**/Pd(BF₄)₂ complex. ORTEP drawings are shown at 50% probability ellipsoids. Colour codes; carbon: grey, nitrogen: blue, oxygen: red, palladium: dark blue. Hydrogen atoms, *p*-anisyl substituents, and counter anions were omitted for clarity.



Scheme 3. Unidirectional Pd²⁺ cation swapping between *i*-TEQ **6b** and TEQ **7b**. Partial ¹H NMR spectra in CDCl₃ (i) *i*-TEQ **6b**/Pd(BF₄)₂; (ii) TEQ **7b**; (iii) *i*-TEQ **6b**/Pd(BF₄)₂ + TEQ **7b** at reflux temperature after 4 h; (iv) *i*-TEQ **6b**; (v) TEQ **7b**/Pd(BF₄)₂; (vi) TEQ **7b**/Pd(BF₄)₂ + *i*-TEQ **6b** at reflux temperature after 4 h.

newly observed peaks corresponded to the free forms of *i*-TEQ **6b** and the TEQ **7b**/Pd(BF₄)₂ complex (Scheme 3, (iii) vs (iv, v)). In contrast, under identical conditions, a mixture of the free form of *i*-TEQ **6b** with the TEQ **7b**/Pd(BF₄)₂ complex displayed virtually no change in ¹H NMR analysis, confirming the unidirectional Pd²⁺ cation swapping from *i*-TEQ **6b** to TEQ **7b** (Scheme 3 (iv,v) vs (vi)). The empirically observed higher stability of the Pd²⁺ complex of TEQ **7b** over that of *i*-TEQ **6b** was reproduced by DFT calculations at the B3LYP-D3/6-31G(d,p)-SDD(Pd)/IEFPCMC(CHCl₃) level of theory; [*i*-TEQ **6b** + TEQ **7b**/Pd²⁺] is 27.7 kcal·mol^{−1} more stable than [*i*-TEQ **6b**/Pd²⁺ + TEQ **7b**].

The photophysical properties of *i*-TEQ **6b** were systematically investigated. Although *i*-TEQ **6b** is inherently barely emissive, the addition of TFA induced a pronounced fluorescence enhancement in an equivalence-dependent manner (Fig. 6). In CH₂Cl₂, the fluorescence intensity of *i*-TEQ **6b** increased progressively with the incremental addition of TFA, reaching a plateau at 4 equivalents (460 nm, Φ_F = 0.41). This acid-responsive fluorescence behaviour,



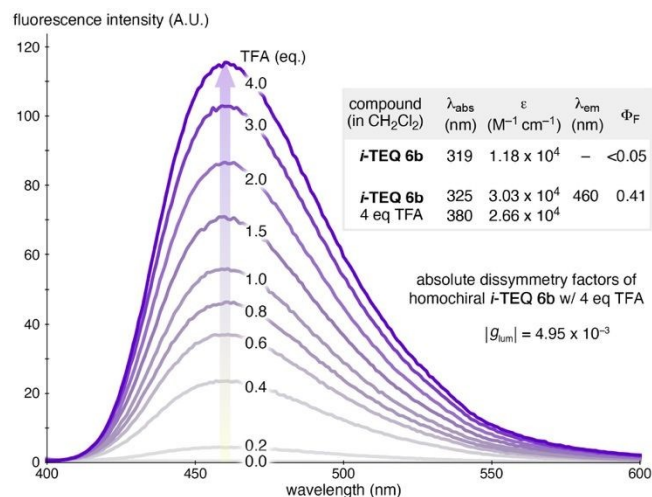
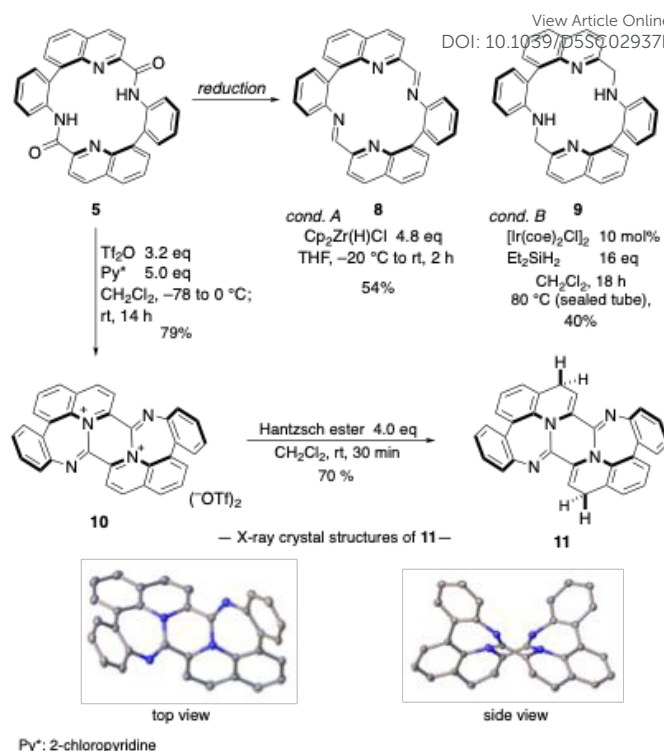


Fig. 6 Photophysical properties of *i*-TEQ 6b. Fluorescence spectra of *i*-TEQ 6b in CH₂Cl₂ (20 μM) were recorded upon incremental addition of TFA in CH₂Cl₂ (excitation at 385.5 nm).

combined with the inherent chirality of **6b**, prompted us to explore its potential in circularly polarized luminescence (CPL). Enantiomerically pure samples of (+)-**6b** and (–)-**6b** exhibited mirror-image CPL spectra upon the addition of 4 equivalents of TFA, with an absolute luminescence dissymmetry factor ($|g_{\text{lum}}|$) of 4.95×10^{-3} .²³ Notably, this value is an order of magnitude greater than that of ring-connectivity isomer **TEQ 7b**,^{6a} highlighting the strong influence of the concatenation pattern on the resultant physicochemical properties.²⁴

Derivatization from cyclic diamide

Cyclic diamide **5**, a key intermediate in the synthesis of *i*-TEQs, serves as a flexible N4 macrocyclic scaffold (Scheme 4). Partial reduction of the amide moiety of **5** using the Zr-based Schwartz reagent²⁵ afforded diimine **8** in 54% yield. Reduction to secondary amines was achieved *via* Ir-catalysed silane conditions,²⁶ affording tetradentate ligand **9**. While electrophilic activation of the amide with Tf₂O followed by formal cycloaddition with alkynes furnishes the quinoline ring *en route* to *i*-TEQs (*vide supra*), a two-fold intramolecular cyclization by the neighbouring quinoline proceeded in the absence of an external nucleophile to afford a warped, tetraaza dicationic π -material **10**. A brief base screening identified electron-deficient 2-chloropyridine as optimal, providing **10** in 79% yield. **10** was readily reduced to furnish a more stable, neutral fused polycyclic material **11**,²⁷ whose unique three-dimensional structure was unambiguously determined by X-ray crystallographic analysis.



Scheme 4. Derivatization from cyclic diamide **5**.

Conclusions

Here, we describe the design and synthesis of a *D*₂-symmetric *iso*-TEtraQuinoline (*i*-TEQ) as an inherently, three-dimensional analogue of porphyrin. *i*-TEQ is a head-to-head quinoline tetramer and a connectivity isomer of previously reported *S*₄-symmetric, achiral **TEQ**, in which four quinoline units are concatenated in a head-to-tail fashion. Comprehensive and systematic comparable analyses of *i*-TEQ and **TEQ** revealed the unique features of these closely related molecular entities in terms of their overall architecture, stereochemical integrity, intrinsic ring strain, metal complexation abilities, and photophysical behaviour. Given its built-in chirality, *i*-TEQ represents a unique molecular scaffold that will serve as a cornerstone in the development of chiral porphyrinoids, thereby expanding the chemical space of porphyrin-based materials.



Author contributions

N. K. and W. X. conceived and directed the project. R. Y. and W. X. synthesised, analysed, and characterised all compounds. T. K. performed theoretical calculations with partial support from N. K. Y. N. carried out CPL measurement and related data analysis. The draft manuscript was written by W. X. and N. K., and all the authors contributed to finalize manuscript through proofreading. All authors approved the final version of the manuscript.

Conflicts of interest

There are no conflicts to declare.

Data availability

Experimental and characterization data, including crystallographic data [**5** (CCDC 2392427), **6b** (CCDC 2392429), and **6d** (CCDC 2392433), **6b**/Pd(BF₄)₂ (CCDC 2392430), **9** (CCDC 2392428)], photophysical measurements, and NMR spectra, as well as computational investigations. The data supporting this article have been included as part of the ESI.

Acknowledgements

This work was financially supported by KAKENHI grant JP22K19037 (Grant-in-Aid for Exploratory Research; to N.K.), JP23H01952 (Grant-in-Aid for Scientific Research (B); to N.K.), and MEXT KAKENHI grant 23H03809 (Grant-in-Aid for Transformative Research Areas (B); to N.K.). N.K. thanks the Mitsubishi Foundation and Mukai Science and Technology Foundation for financial support. W.X. thanks TOBE MAKI foundation for financial support. T.K. thanks Izumi-zaidan for financial support. Dr. Tomoyuki Kimura at the Institute of Microbial Chemistry is gratefully acknowledged for X-ray crystallographic analysis.

Notes and references

- (a) Y.-B. Wang and B. Tan, *Acc. Chem. Res.*, 2018, **51**, 534–547; (b) J. K. Cheng, S.-H. Xiang, S. Li, L. Ye and B. Tan, *Chem. Rev.*, 2021, **121**, 4805–4902; (c) G.-J. Mei, W. L. Koay, C.-Y. Guan and Y. Lu, *Chem*, 2022, **8**, 1855–1893.
- (a) L. Pu, *Chem. Rev.*, 1998, **98**, 2405–2494; (b) L. Pu, *Acc. Chem. Res.*, 2012, **45**, 150–163.
- (a) G. Bringmann, T. Gulder, T. A. M. Gulder and M. Breuning, *Chem. Rev.*, 2011, **111**, 563–639; (b) S. R. LaPlante, L. D. Fader, K. R. Fandrick, D. R. Fandrick, O. Hucke, R. Kemper, S. P. F. Miller and P. J. Edwards, *J. Med. Chem.*, 2011, **54**, 7005–7022; (c) M. Basilaia, M. H. Chen, J. Secka and J. L. Gustafson, *Acc. Chem. Res.*, 2022, **55**, 2904–2919; (d) B. A. Lanman, A. T. Parsons and S. G. Zech, *Acc. Chem. Res.*, 2022, **55**, 2892–2903; (e) Z. Wang, L. Meng, X. Liu, L. Zhang, Z. Yu and G. Wu, *Eur. J. Med. Chem.*, 2022, **243**, 114700.
- For selected reviews on asymmetric catalysis with 1,1'-bi-2-naphthol (BINOL); (a) Y. Chen, S. Yekta and A. K. Yudin, *Chem. Rev.*, 2003, **103**, 3155–3212; (b) L. Eberhardt, D. Armspach, J. Harrowfield and D. Matta, *Chem. Soc. Rev.*, 2008, **37**, 839–864; (c) P. W. N. M. van Leeuwen, P. C. J. Kamer, C. Claver, O. Pàmies and M. Diéguez, *Chem. Rev.*, 2011, **111**, 2077–2118; (d) D. Parmar, E. Sugiono, S. Raja and M. Rueping, *Chem. Rev.*, 2014, **114**, 9047–9153; (e) L. Pu, *Chem. Rev.*, 2024, **124**, 6643–6689. For lanthanum–lithium–BINOL (LLB) complexes; (f) M. Shibasaki and N. Yoshikawa, *Chem. Rev.*, 2002, **102**, 2187–2210; (g) N. Kumagai, M. Kanai and H. Sasai, *ACS Catal.*, 2016, **6**, 4699–4709. For the other phosphines, amides, and others; (h) Q.-H. Fan, Y.-M. Li and A. S. C. Chan, *Chem. Rev.*, 2002, **102**, 3385–3466; (i) M. Berthod, G. Mignani, G. Woodward and M. Lemaire, *Chem. Rev.*, 2005, **105**, 1801–1836; (j) T. Akiyama and K. Mori, *Chem. Rev.*, 2015, **115**, 9277–9306; (k) H. Ni, W.-L. Chan and Y. Lu, *Chem. Rev.*, 2018, **118**, 9344–9411; For 1,1'-binaphthyl-based macrocycles; (l) R. Ning, H. Zhou, S.-X. Nie, Y.-F. Ao, D.-X. Wang and Q.-Q. Wang, *Angew. Chem. Int. Ed.*, 2020, **59**, 10894–10898; (m) G. Sun, X. Zhang, Z. Zheng, Z.-Y. Zhang, M. Dong, J. L. Sessler and C. Li, *J. Am. Chem. Soc.*, 2024, **146**, 26233–26242.
- (a) P. R. Blakemore, C. Kilner and S. D. Milicevic, *J. Org. Chem.*, 2006, **71**, 8212–8218; (b) J. Xiao and T.-P. Loh, *Org. Lett.*, 2009, **11**, 2876–2879; (c) S.-M. Sephton, C. Wang, L. N. Zakharov and P. R. Blakemore, *Eur. J. Org. Chem.*, 2012, 3249–3260; (d) J. V. Chocholoušová, J. Vacek, A. Andronova, J. Mišek, O. Songis, M. Šámal, I. G. Stará, M. Meyer, M. Bourdillon, L. Pospíšil and I. Starý, *Chem. Eur. J.*, 2014, **20**, 877–893.
- (a) W. Xu, Y. Nagata and N. Kumagai, *J. Am. Chem. Soc.*, 2023, **145**, 2609–2618. Other examples of quinoline-based macrocycles; (b) P. S. Shirude, E. R. Gillies, S. Ladame, F. Godde, K. Shin-ya, I. Huc and S. Balasubramanian, *J. Am. Chem. Soc.*, 2007, **129**, 11890–11891; (c) T. Shimasaki, R. Kuroda, M. Akao, T. Akimoto, T. Ishikawa, T. Iwanaga, N. Teramoto and M. Shibata, *Chem. Lett.*, 2019, **48**, 133–136; (d) S. Adachi, M. Shibasaki and N. Kumagai, *Nat. Commun.*, 2019, **10**, 3820; (e) D. Yang, J. L. Greenfield, T. K. Ronson, L. K. S. von Krbek, L. Yu and J. R. Nitschke, *J. Am. Chem. Soc.*, 2020, **142**, 19856–19861; (f) T. Kobayashi and N. Kumagai, *Angew. Chem. Int. Ed.*, 2023, **62**, e202307896; (g) T. Kobayashi, T. Sakurai and N. Kumagai, *Bull. Chem. Soc. Jpn.*, 2023, **96**, 1139–1143; (h) K. Kihara, T. Kobayashi, W. Xu and N. Kumagai, *Chem. Eur. J.*, 2024, **30**, e202304176; (i) T. Karimata, W. Xu and N. Kumagai, *Chem. Eur. J.*, 2025, **31**, e202404335.
- M. Nishiwaki, W. Xu and N. Kumagai, *Asian J. Org. Chem.*, 2023, **12**, e202300261.
- For the naphthalene analogue; (a) Y. Nojima, M. Hasegawa, N. Hara, Y. Imai and Y. Mazakia, *Chem. Commun.*, 2019, **55**, 2749–2752; (b) Y. Nojima, M. Hasegawa, N. Hara, Y. Imai and Y. Mazaki, *Chem. Eur. J.*, 2021, **27**, 5923–5929.
- For other inherently chiral macrocyclic compounds, see: (a) S. Tong, J.-T. Li, D.-D. Liang, Y.-E. Zhang, Q.-Y. Feng, X. Zhang, J. Zhu and M.-X. Wang, *J. Am. Chem. Soc.*, 2020, **142**, 14432–14436; (b) H. Han, X.-G. Wang, S. Tong, J. Zhu and M.-X. Wang, *ACS Catal.*, 2025, **15**, 6018–6024; (c) S. J. Nemat, H. Jędrzejewska, A. Prescimone, A. Szumna and K. Tiefenbacher, *Org. Lett.*, 2020, **22**, 5506–5510; (d) G. E. Arnott, *Chem. Eur. J.*, 2018, **24**, 1744–1754; (e) F. Sannicolò, P. R. Mussini, T. Benincori, R. Cirilli, S.



- Abbate, S. Arnaboldi, S. Casolo, E. Castiglioni, G. Longhi, R. Martinazzo, M. Panigati, M. Pappini, E. Q. Procopio and S. Rizzo, *Chem. Eur. J.*, 2014, **20**, 15298–15302.
10. A. Suzuki, *Angew. Chem., Int. Ed.*, 2011, **50**, 6722–6737.
11. See Supplementary Information Section 2-6 for details.
12. M. Movassaghi and M. D. Hill, *J. Am. Chem. Soc.*, 2006, **128**, 14254–14255.
13. See Supplementary Information Section 2-9 and 2-10 for details.
14. X-ray crystallographic analysis of **i-TEQ 6b** and **TEQ 7b** revealed that crystal structures and calculated structures of the main frameworks are almost identical.
15. A. Okuniewski, D. Rosiak, J. Chojnacki and B. Becker, *Polyhedron*, 2015, **90**, 47–57.
16. See Supplementary Information Section 7-7 for details.
17. C. E. Colwell, T. W. Price, T. Stauch and R. Jasti, *Chem. Sci.*, 2020, **11**, 3923–3930.
18. See Supplementary Information Figure S28–S29.
19. See Supplementary Information Table S4 for details.
20. See Supplementary Information Figure S17–S18.
21. See Supplementary Information Section 5-3 for details.
22. See Supplementary Information Section 6 for details.
23. G. Longhi, E. Castiglioni, J. Koshoubu, G. Mazzeo, S. Abbate, *Chirality*, 2016, **28**, 696–707. See Supplementary Information Section 7-5 for experimental details.
24. See Supplementary Information Section 7-6 for calculational details.
25. J. Schwartz and J.A. Labinger, *Angew. Chem. Int. Ed.*, 1976, **15**, 333–340.
26. C. Cheng and M. Brookhart, *J. Am. Chem. Soc.*, 2012, **134**, 11304–11307.
27. For fused polycyclic material see following reviews or latest articles; (a) H. Ito, K. Ozaki and K. Itami, *Angew. Chem. Int. Ed.*, 2017, **56**, 11144–11164; (b) S. H. Pun and Q. Miao, *Acc. Chem. Res.*, 2018, **51**, 1630–1642; (c) G. G. Miera, S. Matsubara, H. Kono, K. Murakami and K. Itami, *Chem. Sci.*, 2022, **13**, 1848–1868; (d) S. M. Elbert, O. T. A. Paine, T. Kirschbaum, M. P. Schuldt, L. Weber, F. Rominger and M. Mastalerz, *J. Am. Chem. Soc.*, 2024, **146**, 27324–27334. For aza-substituted warped nano-sheets; (e) S. Ito, Y. Tokimaru and K. Nozaki, *Angew. Chem. Int. Ed.*, 2015, **54**, 7256–7260; (f) H. Yokoi, Y. Hiraoka, S. Hiroto, D. Sakamaki, S. Seki and H. Shinokubo, *Nat. Commun.*, 2015, **6**, 8215; (g) S. Higashibayashi, P. Pandit, R. Haruki, S. Adachi and R. Kumai, *Angew. Chem. Int. Ed.*, 2016, **55**, 10830–10834; (h) K. Oki, M. Takase, S. Mori, A. Shiotari, Y. Sugimoto, K. Ohara, T. Okujima and H. Uno, *J. Am. Chem. Soc.*, 2018, **140**, 10430–10434; (i) T. Kirschbaum, F. Rominger and M. Mastalerz, *Chem. Eur. J.*, 2020, **26**, 14560–14564; (j) P. An, R. Li, B. Ma, R.-Y. He, Y.-K. Zhang, M.-J. Xiao and B. Zhang, *Angew. Chem. Int. Ed.*, 2021, **60**, 24478–24483; (k) J. Wagner, P. Z. Crocorno, M. A. Kochman, A. Kubas, P. Data and M. Lindner, *Angew. Chem. Int. Ed.*, 2022, **61**, e202202232; (l) M. Krzeszewski, Ł. Dobrzycki, A. L. Sobolewski, M. K. Cyrański and D. T. Gryko, *Chem. Sci.*, 2023, **14**, 2353–2360.

View Article Online
DOI: 10.1039/D5SC02937F



Experimental and characterization data, including crystallographic data [**5** (CCDC 2392427), **6b** (CCDC 2392429), and **6d** (CCDC 2392433), **6b**/Pd(BF₄)₂ (CCDC 2392430), **9** (CCDC 2392428)], photophysical measurements, and NMR spectra, as well as computational investigations. The data supporting this article have been included as part of the ESI.

